Journal of the Australian Ceramic Society (2019) 55:1187–1194
https://doi.org/10.1007/s41779-019-00335-5

RESEARCH

Dielectric and magnetic properties of $BaFe_{11.7}Ni_{0.3}O_{19}$ (BHNF) ceramic synthesized by chemical route

Atendra Kumar[1] · Shiva Sundar Yadava[1] · Pooja Gautam[1] · Ankur Khare[1] · Laxman Singh[2] · K. D. Mandal[1]

Received: 2 January 2018 / Revised: 6 February 2019 / Accepted: 5 March 2019 / Published online: 1 April 2019

Abstract

Nickel-doped barium hexaferrite, $BaFe_{11.7}Ni_{0.3}O_{19}$ (BHNF), ceramic was prepared by a chemical route. The single phase formation of BHNF ceramic in the sintered material at 1200 °C for 6 h was confirmed by powder XRD. Hexagonal and round shape particles were observed by transmission electron microscopy (TEM), and the particle size was found to be 81 ± 10 nm. The average roughness and root mean square roughness were observed by atomic force microscopy (AFM) evaluated to be 57 and 73 nm, respectively. The zero field cooled (ZFC), field cooled (FC), and magnetic hysteresis curves indicate temperature dependent ferromagnetic behavior of BHNF ceramic. The dielectric constant (ε') was determined to be 1.7×10^4 at 423 K and 100 Hz. The high value of ε' indicates the presence of semiconducting grains and insulating grain boundaries which was supported by internal barrier layer capacitance mechanisms.

Keywords Chemical route · FT-IR · Magnetic behavior · Dielectric properties

Introduction

Barium hexaferrite with chemical composition, $MFe_{12}O_{19}$ (M = Ba, Sr or Pb), have considerable attention in electronic applications such as permanent magnet, high-density magnetic recording media, microwave device, and telecommunications equipment. These important applications of this material are due to strong uniaxial crystalline anisotropy, high saturated magnetic polarization, large coercivity, and high resonant frequency with an excellent capability and corrosion resistance [1–3]. The large crystal anisotropy and high intrinsic coercivity of this material are responsible for high stability and electrical resistivity. The hexaferrite ($BaFe_{12}O_{19}$) have M-type structure which exhibits strong ferromagnetism among ferrites. It was widely used in electronic device, and their properties strongly depend on microstructure and morphology. These materials have high relevance in higher frequency and high resistance to the heat and corrosion than others due to high coercivity with small particle size [4]. The magnetic and dielectric properties of ferrites have been strongly influenced by synthesis procedures and substitution of various cations such as divalent and trivalent [5]. The various synthesis methods for the fabrication of M-type hexaferrite ceramic has been used, such as ceramic method [6], citrate auto-combustion synthesis [7], co-precipitation [8], mechano-thermal treatment [9], sol-gel, microemulsion techniques [10], ball milling [11], wet mixing method [12], and hydrothermal [13]. The substitution of divalent and tetravalent (Co^{+2}, Ni^{+2}, Ti^{+4}) cations at the site of Fe^{+3} and Ba have been carried out for the improvement of magnetic properties [14, 15]. These improvements have occurred because of their similarity in ionic radii and their electronic configuration. Their magnetic properties may be conjointly enhanced by the substitution of Fe^{+3} with magnetic or non-magnetic ions which result in significant change in saturation magnetization because of modification within the net magnetic moment per molecules [16–19]. The substitution of Mn^{+3}, La^{+3}, Co^{+2}-Zr^{+4}, Ti^{+4}-Mn^{+4}, and Co^{+2}-Ti^{+4} ions have been decreased in saturation magnetization (Ms) and coercivity (Hc) [20]. This decrease is due to the presence of secondary phase which also inhibits the recording application of material. Most of the works have been carried out for the synthesis and characterization of M-type barium hexaferrite, for examples $BaFe_{12}O_{19}$, $BaMe_xFe_{12-x}O_{19}$ (Me^{+3} = Al, Cr, Bi, Sc), $BaMe_xIr_xFe_{12-2x}O_{19}$

✉ K. D. Mandal
kdmandal.apc@itbhu.ac.in

[1] Department of Chemistry, Indian Institute of Technology, Banaras Hindu University, Varanasi, U.P. 221005, India

[2] Department of Chemistry, University of Ulsan, 93 Daehak-ro Nam-gu, Ulsan 680-749, Republic of Korea

(Me^{+2} = Co, Zn), $BaZn_xSn_xFe_{12-2x}O_{19}$, $BaCo_xRu_xFe_{12-2x}O_{19}$, $BaMe_xTi_xFe_{11.6-2x}O_{19}$ (Me^{+2} = Co, Zn), and $BaMe_xTi_xFe_{12-2x}O_{19}$ (Me^{+2} = Co, Zn, Mn) [21].

In the present study, we studied the effect of Ni^{+2} substitutions for the improvement of electrical and magnetic properties of $BaFe_{12}O_{19}$ ceramic synthesized by chemical route. The chemical route is more suitable than other synthesis methods for the preparation of nanostructured materials. It was observed that substituting Fe^{+3} by Ni^{+2} ions reduces coercivity and saturation magnetization which is a major factor for recording data [22].

Experimental

Material synthesis

Nickel-doped barium hexaferrite was synthesized by the chemical route using analytical grade chemicals, $Ba(NO_3)_2$ (99% Merck, India), $Fe(NO_3)_3$, $9H_2O$ (98% Merck, India), and $Ni(NO_3)_2$ (99% Merck, India) as starting materials. The stoichiometric amount of metal nitrates was dissolved in deionized distilled water along with the appropriate amount of citric acid ($C_6H_8O_7$. H_2O, 99% Merck, India) as per equivalent to the metal ions. The resulting solution was heated on a hot plate with magnetic stirrer at 70–80 °C to evaporate excesses water. On further heating, a fluffy mass was obtained which burns with a sooty flame. The obtained porous ash was crushed into fine powder with the help of mortar and pestle. The resultant dry powder was calcined at 800 °C for 8 h in the electrical muffle furnace after that cylindrical pellets (13.0 mm diameters, 1.6 mm thicknesses) was prepared using 2 wt% polyvinyl alcohol (PVA) as a binder. These pellets were sintered at 1200 °C for 6 h and further used for different physiochemical characterizations such as XRD, SEM, TEM, EDX, and AFM.

Characterization

The crystalline phase of sintered BHNF ceramic was identified by X-ray diffraction analysis (Rigakuminiflex 600, Japan) employing Cu-Kα radiation ($\lambda = 1.54$ Å). The microstructure and elemental analysis of the BHNF were observed by scanning electron microscope (ZEISS, model EVO–18 research; Germany) and energy-dispersive X-ray spectroscopy (EDX, Oxford instrument; USA), respectively. Transmission electron microscope (TEM, FEI TECANI G^2 20 TWIN; USA) was used for particle size determination. The surface morphology was examined by atomic force microscopy (NTEGRA Prima, Germany). The ferroelectric properties of the sintered BHNF ceramic were measured by ferroelectric tracer (Automatic P-E loop tracer, Marin India). Magnetic behavior and temperature dependence zero field cooled (M^{ZFC}), field cooled (M^{FC}) over a temperature range 5–300 K and applied a magnetic field 2 T (± 2 T) were recorded by Quantum Design MPMS-3 and SQUID VSM dc magnetometer respectively. The frequency and temperature dependence dielectric of silver coated pellets were carried out using LCR meter (PSM 1735, NumetriQ 4th Ltd. U.K.).

Results and discussion

Crystallinity and microstructural studies

XRD patterns of BHNF ceramic calcined at 800 °C for 8 h and sintered at 1200 °C for 6 h, respectively are shown in Fig. 1. The single phase formation of the hexagonal BHNF ceramic is confirmed at 1200 °C for heating up to 6 h. The diffraction patterns are matched with JCPDS card no. (78–0132) along with small impurity of Fe_2O_3 (JCPDS card no. 89–7047). The average crystallite size is calculated by the Debye–Scherrer formula [23].

$$D = k\lambda/\beta\cos\theta \quad (1)$$

where, D is the crystallite size, k is a constant value taken as 0.96, λ is the wavelength of X-ray, θ is the Bragg angle of peaks, and β represents full width at half maxima (FWHM). The average crystallite size of BHNF ceramic is found to be 30 ± 5 nm. To understand the functional group of BHNF ceramic, FTIR spectrum recorded in the frequency range 500–2000 cm^{-1} is shown in Fig. 2. There are two absorption peaks observed in the frequency range in between 500 and 800 cm^{-1} which is associated with Fe–O stretching vibration bands due

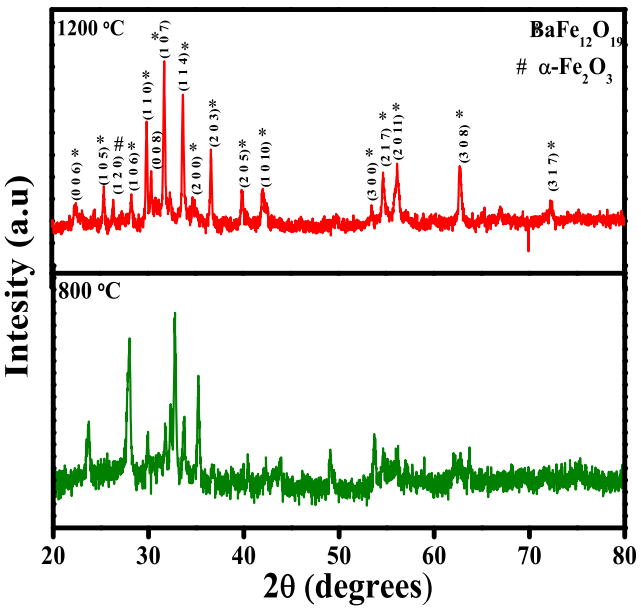

Fig. 1 Shows XRD diffraction patterns of $BaFe_{11.7}Ni_{0.3}O_{19}$ ceramic **a** calcined at 800 °C for 8 h **b** sintered at 1200 °C for 6 h

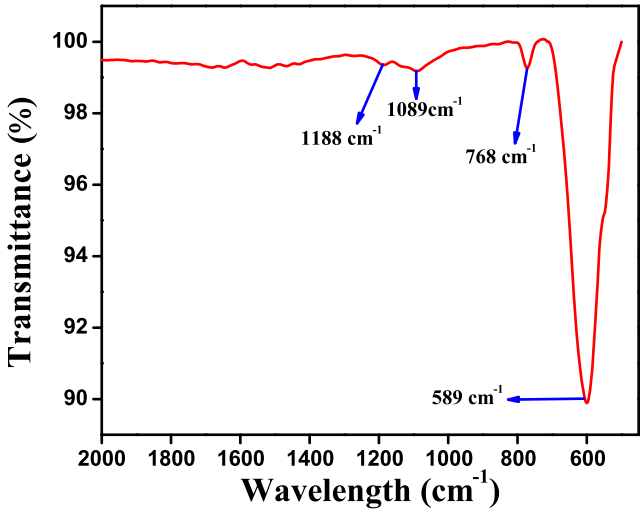

Fig. 2 FTIR spectra of $BaFe_{11.7}Ni_{0.3}O_{19}$ ceramic sintered at 1200 °C for 6 h

to octahedral and tetrahedral sites [24]. The absorption peaks are attributable to metal–oxygen–metal bonds such as Fe–O–Fe bonds, are also found in the frequency ranges 1100–1500 cm^{-1}. The observed absorption peaks confirm the formation of hexaferrite [8].

The bright field TEM images of BHNF ceramic sintered at 1200 °C for 6 h is shown in Fig. 3a, which reveals the presence of hexagonal and round shape particles of size 81 ± 10 nm. With the help of SAED patterns, the zone axis containing (3 0 13), (1 1 10), and (1 1 10), (0 0 10) planes are calculated to be ($1\bar{3}\ 1\bar{7}\ 3$) and ($10\ 1\bar{0}\ 0$), respectively as shown in Fig. 3b. Figure 3c shows the high resolution (HR–TEM) image showing the corresponding planes (1 0 7) and (1 1 2) having d-spacing 0.271 and 0.286 nm, respectively. All the indexed planes obtained by HR-TEM and SAED pattern are in good agreement with XRD results which confirmed the hexagonal nature of the material. Figure 4a shows hexagonal plate-like grains which are separated by well-defined grain boundaries. The average grain size is found to be 620 ± 10 nm which is larger than crystallite as well as particle size due to crystallites are formed by combination of few particles whereas grains by agglomeration. The pH of the solution also affected on the morphology of the particles of the barium hexaferrite as a result of which particle size will increase with the decrease of pH which can ensure to decrease within the rate of growth or increasing the nucleation rate of the particles. The EDX spectra of BHNF ceramic indicates the presence of Ba, Fe, Ni, and O elements as shown in Fig. 4b. The atomic percentages of Ba, Fe, Ni, and O are found to be 21.74, 53.79, 3.23, and 21.24, respectively. Figure 4c–f shows energy dispersive mapping which indicates the

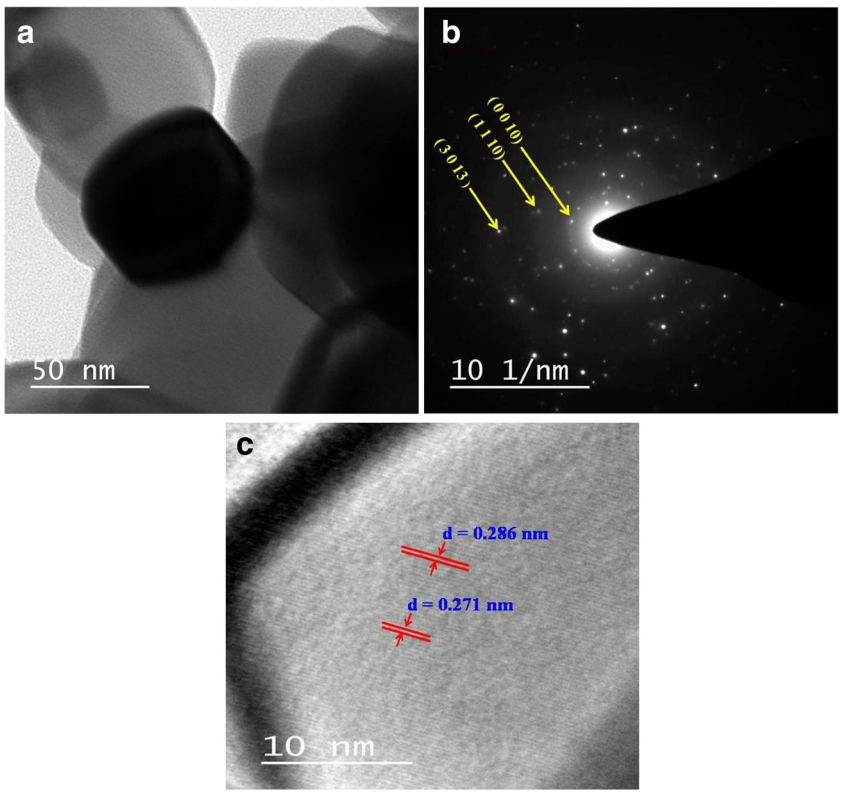

Fig. 3 **a** Bright field TEM image **b** selected area diffraction (SAED) pattern **c** High-resolution TEM image of $BaFe_{11.7}Ni_{0.3}O_{19}$ ceramic

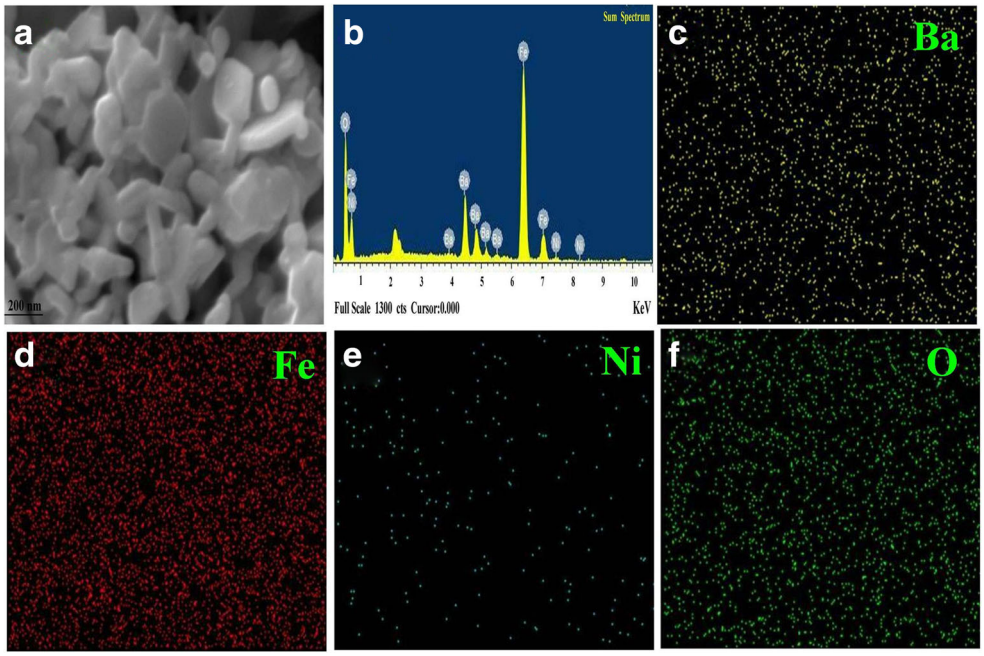

Fig. 4 **a** SEM image, **b** EDX spectra, and **c–f** elemental mapping of each elements corresponding to $BaFe_{11.7}Ni_{0.3}O_{19}$ ceramic

homogeneous distribution of the corresponding elements in BHNF ceramic.

Figure 5a represents the two-dimensional AFM image of BHNF ceramic sintered at 1200 °C for 6 h; the surface morphology reveals the homogenous distribution of grains is separated by grain boundaries. The three-dimensional image of BNHF ceramic is shown in Fig. 5b**;** after a thorough analysis of the grains, we observed the average roughness (R_a), root mean square roughness (R_q), maximum area peak height (Sp), and maximum peak-valley depth are 57 nm, 73 nm, 250 nm, and 329 nm, respectively. Figure 5c shows the histogram of grain size which indicates that the majority of grains are in the range of 800–1000 nm, whereas the average grain size is found to be 630 nm which is supported by SEM. Figure 5d shows peak distribution curve for grain roughness of BHNF ceramic [25]. The polarization versus electric field (P–E) hysteresis loop of BHNF ceramic measured at room temperature is shown in Fig. 6 which indicates the absence of saturation in the P–E curve. The measured values of remnant polarization (P_r) and coercivity (E_c) are obtained from the curve and found to be 0.0125 μC/cm^2 and 3.46 kV/cm. The ferroelectricity of material is because of the distinction in ionic radii of host permittivity and impurity of cations. Ni^{+2} cations reduce the off-center effect of FeO_6 octahedra and also suppress the oxygen vacancy which enhanced the ferroelectric behavior. The absence of saturation polarization (P_s) is explained due to the lossy capacitor nature of these materials [26, 27].

Magnetic studies

The variation of magnetization with temperature at constant applied magnetic field of 100 Oe of the BHNF ceramic is shown in Fig. 7a. The observed magnetization (ZFC and FC) increases gradually with decrease in temperature. The ZFC curve shows a hump at 172 K which indicates blocking temperature (T_b) as shown in inset Fig. 7a. At this temperature, most of the spins are blocked in the material. The observed value of T_b is considerably low in comparison to the previously reported value [28]. This low value of T_b is favorable for biomedical applications in magnetic hyperthermia. Figure 7b represents the M–H hysteresis loop of BHNF ceramic at 5 K and 300 K recorded at ± 2 T. The saturation magnetization (M_s) and remnant magnetization (M_r) decreases with increasing temperature. This inverse behavior of magnetization with temperature is due to the existence of spin canting and superexchange interaction of Fe^{3+}–O^{2-}–Fe^{3+} on the substitution of Ni^{+2} ions in $BaFe_{12}O_{19}$ ceramic [29]. The lower values of coercivity (H_c) of the BHNF ceramic as compared with barium hexaferrite is due to the presence of unsymmetrical hexagonal particles as reported in earlier [30].The decrease in coercivity of nickel-doped barium hexaferrite may be due to reduction in rate of the magneto-crystalline anisotropy (K) with increasing the concentration of Ni [31]. The low values of "K" enhance the conductivity of the materials which is useful for sensor, transducers, and catalysts. The saturation magnetization is found to be 52.860 and 37.135 emu/g for 5 K and 300 K, respectively. The squareness ratio (M_r/M_s) values for BHNF ceramic are near to 0.5 at room

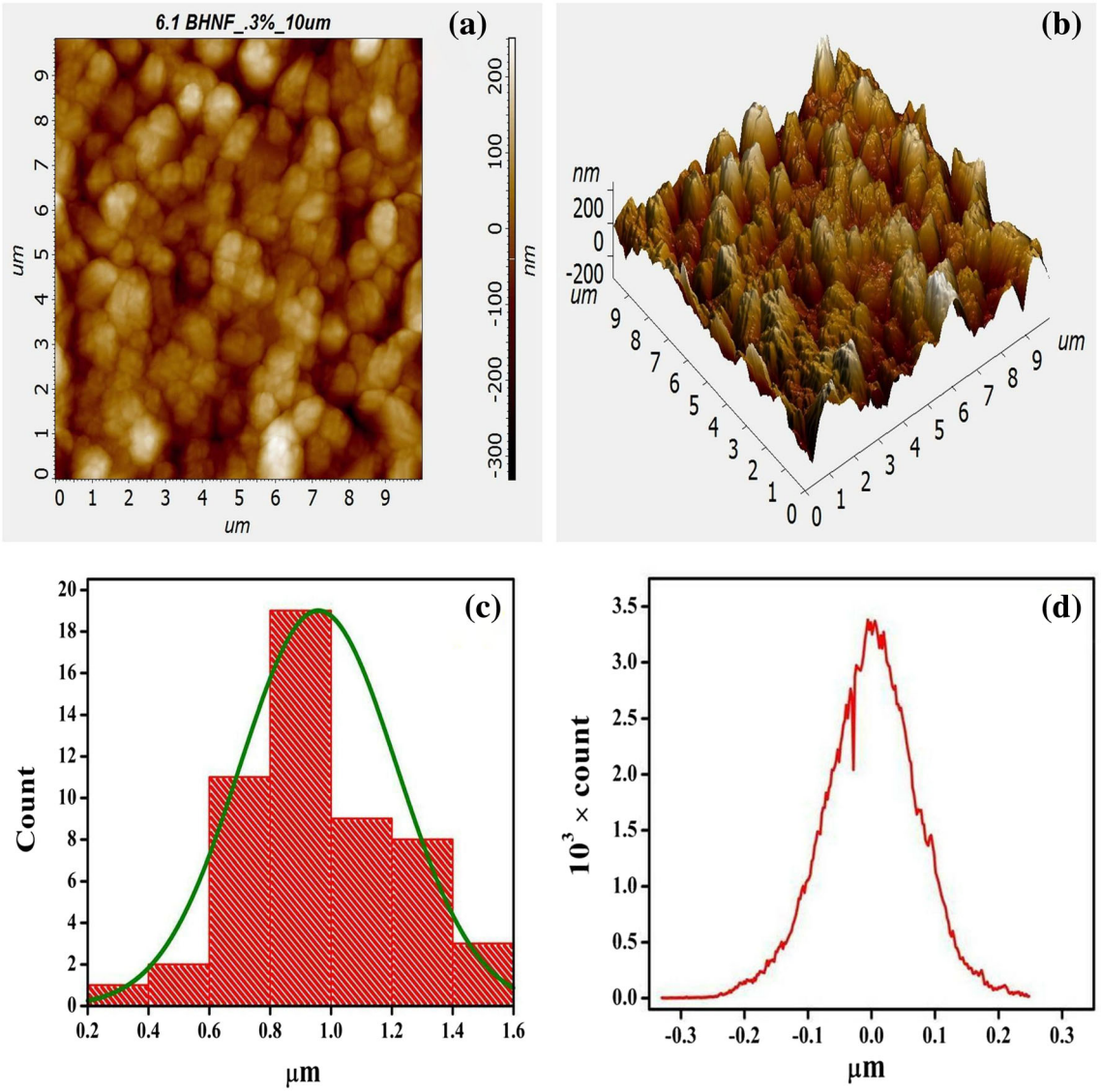

Fig. 5 AFM images of $BaFe_{11.7}Ni_{0.3}O_{19}$ ceramic **a** two dimensional image for grain boundary, **b** three dimensional for surface roughness, **c** bar diagram for particle size distribution, and **d** depth histogram graph

temperature. The lower value of M_r/M_s suggests that BHNF ceramic having a single domain, noninteracting particles which are randomly oriented, exhibit hard magnetic properties [32]. The magnetic parameters for BHNF ceramic obtained from hysterias loop at two temperatures are mentioned in Table 1.

Dielectric studies

Figure 8 shows the dielectric constant (ε') and dielectric loss (tan δ) with the temperature at few selected frequencies. The relaxation peaks are observed at all measured frequencies and shifted towards higher temperature as shown in Fig. 8a, which may be due to the presence of oxygen vacancies in BHNF ceramic. The value of dielectric constant is found to be 1.5×10^4 at 100 Hz [33]. Figure 8b shows temperature dependent dielectric loss at few selected frequencies. The observed dielectric loss remains constant from the temperature (300–405 K) and increases with increasing temperature. This increment in tan δ with higher temperature and lower frequencies may be due to interfacial charge polarization at phase boundaries. The values of tan δ at room temperature are found to be 0.87 for 100 Hz, 1 kHz, 10 kHz, and 100 kHz, respectively.

The effect of frequency on the dielectric constant (ε') and dielectric loss (tan δ) is measured in the temperature range 303–423 K at an interval of 60 degrees are shown in Fig. 9. It is observed from Fig. 9a that the value of dielectric constant decreases with increasing frequency and is almost constant towards higher frequency, due to reversibility of electric field which takes place so rapidly. The value of ε' is found to be 1.7×10^4 at 423 K and 100 Hz. The higher value of dielectric

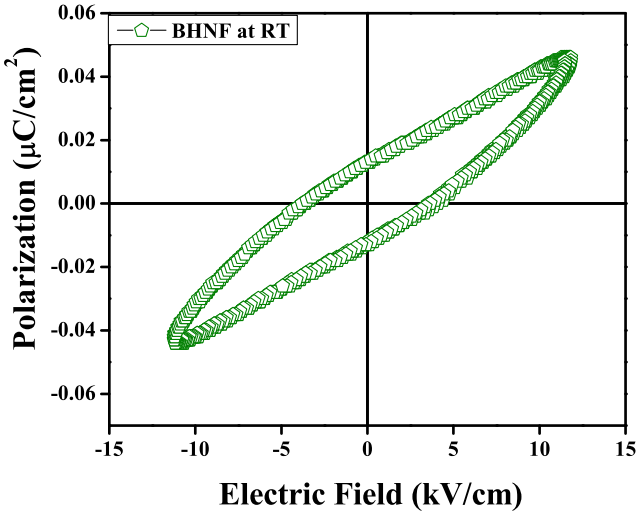

Fig. 6 The polarization verses electric field (P–E) hysteresis loop of $BaFe_{11.7}Ni_{0.3}O_{19}$ ceramic at room temperature

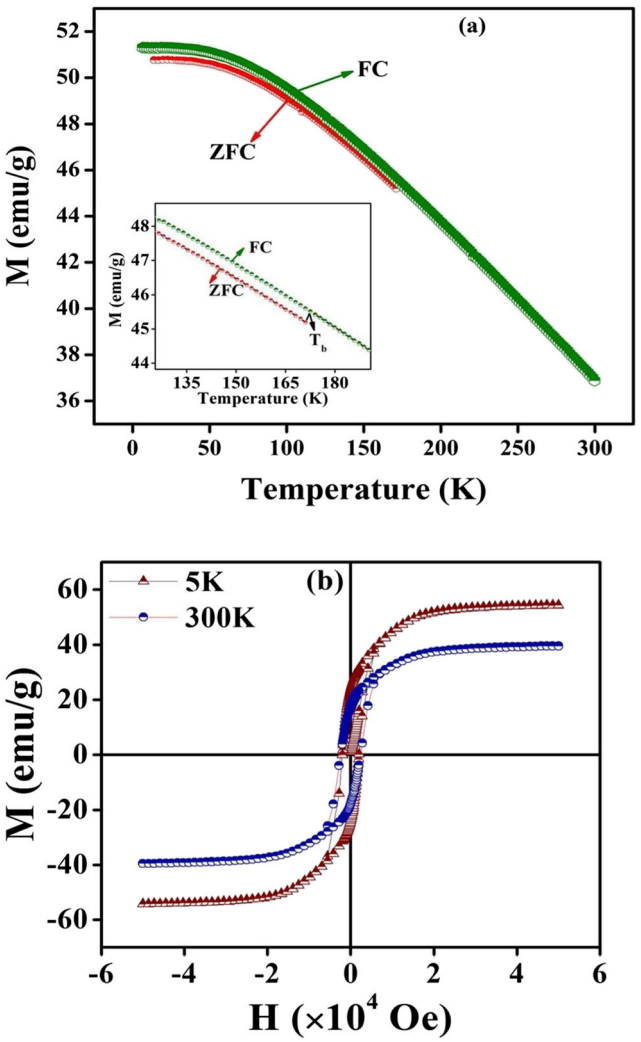

Fig. 7 **a** The variation of magnetization with temperature at constant applied magnetic field of 100 Oe, **b** M-H hysteresis loop recorded at ±2 T of the BHNF ceramic

Table 1 Magnetic parameters of $BaFe_{11.7}Ni_{0.3}O_{19}$ (BHNF) ceramic at different temperature

T (K)	M_s (emu/g)	M_r (emu/g)	M_r/Ms	Hc (A/m)
5	52.868	25.258	0.477	1.55×10^5
300	37.135	18.233	0.491	1.83×10^5

constant at lower frequency may be due to the interfacial charge polarization between semiconducting grains as well as insulating grain boundaries which is supported by internal barrier layer capacitance (IBLC) mechanism [34–36]. The temperature dependent dielectric loss (tan δ) with frequency of BHNF ceramic is shown in Fig. 9b. The values of tan δ increase with the increase of temperature and are almost independent in higher frequency. The Debye-type relaxation peaks are occurring in low-frequency side indicates thermally active relaxation behavior which is suppressed at higher frequency 10^5 Hz [37–39]. The value of tan δ is found to be 3.3 at 423 K and 100 Hz.

Conclusion

BHNF ceramic nanostructured materials have been successfully synthesized by a chemical route. XRD confirmed the formation of phase of BHNF at 1200 °C with a minor phase of Fe_2O_3. BHNF ceramic shows excellent dielectric and magnetic properties over a wide range of temperature. The value of dielectric constant (ε') is found to be 1.7×10^4 at 423 K and

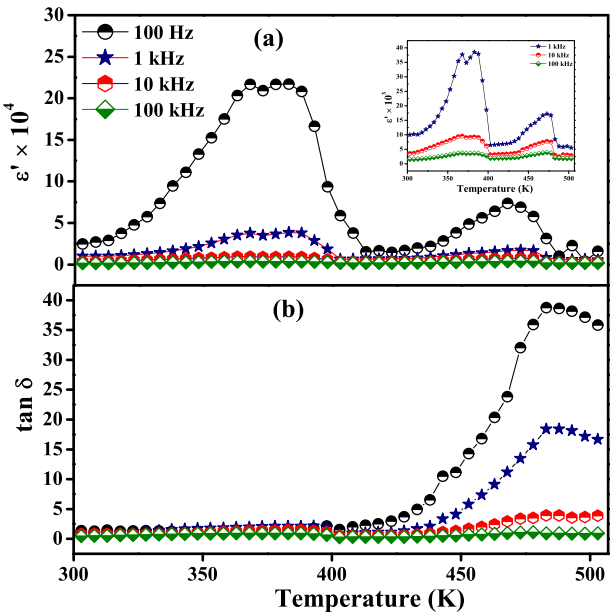

Fig. 8 **a** Dielectric constant (ε') and **b** dielectric loss (tan δ) as a function of temperature at few selected frequencies

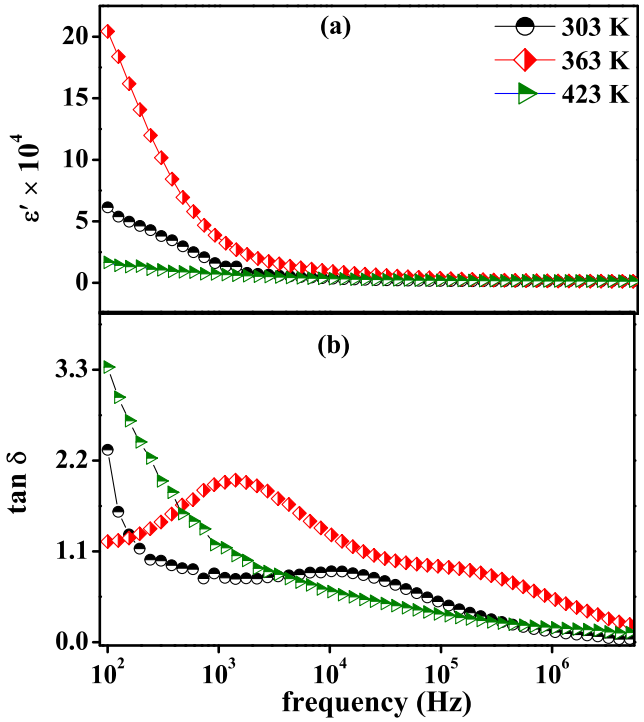

Fig. 9 Frequency dependent **a** dielectric constant (ε') and **b** dielectric loss (tan δ) at few selected temperatures

100 Hz. Ferromagnetic to paramagnetic transitions observed on increasing temperature. The less squareness (M_r/M_s) ratio indicates the presence of monodomain crystal structure and justifies its suitability in various applications such as high magnetic recording media and permanent magnet.

Acknowledgements Authors would like to thank the Central Instrument Facility Center (CIFC) IIT (BHU) for providing SEM, TEM, and MPMS facilities.

References

1. Singhal, S., Namgyal, T., Singh, J., Chandra, K., Bansal, S.: A comparative study on the magnetic properties of $MFe_{12}O_{19}$ and $MAlFe_{11}O_{19}$ (M = Sr, Ba and Pb) hexaferrites with different morphologies. Ceram. Int. **37**(6), 1833–1837 (2011)
2. Onreabroy, W., Papato, K., Rujijanagul, G., Pengpat, K., Tunkasiri, T.: Study of strontium ferrites substituted by lanthanum on the structural and magnetic properties. Ceram. Int. **38**, S415–S419 (2012)
3. Zhang, X., Duan, Y., Guan, H., Liu, S., Wen, B.: Effect of doping MnO_2 on magnetic properties for M-type barium ferrite. J. Magn. Magn. Mater. **311**(2), 507–511 (2007)
4. Pereira, F.M.M., Santos, M.R.P., Sohn, R.S.T.M., Almeida, J.S., Medeiros, A.M.L., Costa, M.M., Sombra, A.S.B.: Magnetic and dielectric properties of the M-type barium strontium hexaferrite ($Ba_xSr_{1-x}Fe_{12}O_{19}$) in the RF and microwave (MW) frequency range. J. Mater. Sci. Mater. Electron. **20**, 408–417 (2009)
5. Ahamed, T.T., Rahaman, I.Z., Rahaman, M.A.: Study on the properties of the copper substituted NiZn ferrites. J. Mater. Process. Technol. **153**, 797–803 (2004)
6. Almeida, M.R., Paragussau, W., Pires, D.S., Correa, R.R., de Araujo Paschoal, C.W.: Impedance spectroscopy analysis of $BaFe_{12}O_{19}$ M-type hexaferrite obtained by ceramic method. Ceram. Int. **35**(6), 2443–2447 (2009)
7. Shirtcliffe, N.J., Thompson, S., O'Keefe, E.S., Appleton, S., Perry, C.C.: Highly aluminium doped barium and strontium ferrite nanoparticles prepared by citrate auto-combustion synthesis. Mater. Res. Bull. **42**(2), 281–287 (2007)
8. Ahmed, A.I., Siddig, M.A., Mirghni, A.A., Omer, M.I., Elbadawi, A.A.: Structural and optical properties of $Mg_{1-x}Zn_xFe_2O_4$ nanoferrites synthesized using co-precipitation method. Advances in Nanoparticles. **4**(02), 45 (2015)
9. Molaeia, M.J., Ataiea, A., Raygan, S., Rahimipour, M.R., Picken, S.J., Tichelaar, F.D., Lagarra, E., Plazola, E.: Magnetic property enhancement and characterization of nano-structured barium ferrite by mechano-thermal treatment. Mater. Charact. **63**, 83–89 (2012)
10. Jotania, R.B., Khomane, R.B., Chauhan, C.C., Menon, S.K., KulKarni, B.D.: Synthesis and magnetic properties of barium-calcium hexaferrite particles prepared by sol-gel and microemulsion techniques. J. Magn. Magn. Mater. **302**(6), 1095–1101 (2008)
11. Molaei, M.J., Ataie, A., Raygan, S., Picken, S.J., Mendes, E., Tichelaar, F.D.: Synthesis and characterization of $BaFe_{12}O_{19}$/Fe_3O_4 and $BaFe_{12}O_{19}$/Fe/Fe_3O_4 magnetic nano-composites. Powder Technol. **221**, 292–295 (2012)
12. Song, S., Song, Q., Li, J., Mudineoalli, V.R., Zhang, Z.: Characterization of submicrometer-sized NiZn ferrite prepared by spark plasma sintering. Ceram. Int. **40**(5), 6473–6479 (2014)
13. Chang, S., Kangning, S., Pengfel, C.: Microwave absorption properties of Ce-substituted M-type barium ferrite. J. Magn. Magn. Mater. **324**(5), 802–805 (2012)
14. Haijun, Z., Zhichao, L., Chenliang, M., Xi, Y., Liangying, Z., Mingzhong, W.: Preparation and microwave properties of Co-and Ti-doped barium ferrite by citrate sol–gel process. Mater. Chem. Phys. **80**(1), 129–134 (2003)
15. Li, Z.W., Ong, C.K., Yang, Z., Wei, F.L., Zhou, X.Z., Zhao, J.H., Morrish, A.H.: Site preference and magnetic properties for a perpendicular recording material: $BaFe_{12-x}Zn_{x/2}Zr_{x/2}O_{19}$ nanoparticles. Phys. Rev. B. **62**(10), 6530–6537 (2000)
16. Mahmood, S.H., Aloqaily, A.N., Maswadeh, Y., Awadallah, A., Bsoul, I., Awawdeh, M., Juwhari, H.: Effects of heat treatment on the phase evolution, structural, and magnetic properties of Mo-Zn doped M-type hexaferrite. Solid State Phenom. **232**, 65–92 (2015)
17. Cao, H., Lu, P., Yu, Z., Chen, J., Wang, S.: Electronic and magnetic properties of vanadium doped AlN nanosheet under in-plane biaxial strains. Superlattice. Microst. **73**, 113–120 (2014)
18. Lu, P., Zhang, X., Cao, H., Yu, Z., Cai, N., Gao, T., Wang, S.: Vanadium doping on magnetic properties of H-passivated ZnO nanowires. J. Mater. Sci. **49**(8), 3177–3182 (2014)
19. Pan, H.: Electronic and magnetic properties of vanadium dichalcogenides monolayers tuned by hydrogenation. J. Phys. Chem. C. **118**(24), 13248–13253 (2014)
20. Iqbal, M.J., Farooq, S.: Suitability of $Sr_{0.5}Ba_{0.5-x}Ce_xFe_{12-y}Ni_yO_{19}$ co-precipitated nanomaterials for inductor applications. J. Alloys Compd. **493**(1), 595–600 (2010)
21. Zhao, W., Zhang, Q., Tang, X., Chenge, H.: Synthesis of nonstoichiometric M-type barium ferrite nanobelt by spark plasma sintering method. Chin. Sci. Bull. **50**(13), 1404–1408 (2005)
22. Rane, M.V., Bahadur, D., Kulkarni, S.D., Date, S.K.: Magnetic properties of NiZr substituted barium ferrite. J. Magn. Magn. Mater. **195**(2), L256–L260 (1999)
23. Singh, L., Rai, U.S., Mandal, K.D.: Preparation and characterization of nanostructured $CaCu_{2.90}Zn_{0.10}Ti_4O_{12}$ ceramic. Nanomaterials and Nanotechnology. **1**, 59–66 (2011)
24. Rostami, M., Moradi, M., Alam, R.S., Mardani, R.: Characterization of magnetic and microwave absorption properties

of multi-walled carbon nanotubes/Mn-Cu-Zr substituted strontium hexaferrite nanocomposites. Mater. Res. Bull. **83**, 379–386 (2016)
25. Gautam, P., Khare, A., Sharma, S., Singh, N.B., Mandal, K.D.: Characterization of $Bi_{2/3}Cu_3Ti_4O_{12}$ ceramics synthesized by semi-wet route. Prog. Nat. Sci. Mater. Int. **26**(6), 567–571 (2016)
26. Awan, S.U., Hasanain, S.K., Anjum, D.H., Awan, M.S., Shah, S.A.: Room temperature p-type conductivity and coexistence of ferro-electric order in ferromagnetic Li doped ZnO nanoparticles. J. Appl. Phys. **116**(16), 164109–164119 (2014)
27. Sarkar, K., Mukherjee, S., Mukherjee, S.: Structural, electrical and magnetic behaviour of undoped and nickel doped nanocrystalline bismuth ferrite by solution combustion route. Processing and Application of Ceramics. **9**(1), 53–60 (2015)
28. Vaishnava, P.P., Senaratne, U., Buc, E., Naik, R., Naik, V.M., Tsoi, G., Wenger, L.E., Boolchand, P.: Magnetic properties of cobalt-ferrite nanoparticles embedded in polystyrene resin. J. Appl. Phys. **99**(8), 08G702–08G704 (2006)
29. Liu, X., Zhong, W., Yang, S., Yu, Z., Gu, B., Du, Y.: Structure and magnetic properties of La^{3+}-substituted strontium hexaferrite particles prepared by sol–gel method. Phys. Status Solidi. **193**(2), 314–319 (2002)
30. Mallick, K.K., Shepherd, P., Green, R.J.: Dielectric properties of M-type barium hexaferrite prepared by co-precipitation. J. Eur. Ceram. Soc. **27**(4), 2045–2052 (2007)
31. Waqar, M., Rafiq, M.A., Mirza, T.A., Khalid, F.A., Khaliq, A., Anwar, M.S., Saleem, M.: Synthesis and properties of nickel-doped nanocrystalline barium hexaferrite ceramic materials. Appl. Phys. A. **124**(4), 286–293 (2018)
32. Mahmood, S.H., Aloqaily, A.N., Maswadeh, Y., Awadallah, A., Bsoul, I., Juwahi, H.: Structural and magnetic properties of Mo-Zn substituted ($BaFe_{12-4x}Mo_xZn_{3x}O_{19}$) M-type hexaferrite. Mat. Sci. Res. India. **11**(1), 09–20 (2014)
33. Bueno, P.R., Ribeiro, W.C., Ramírez, M.A., Varela, J.A., Longo, E.: Separation of dielectric and space charge polarizations in $CaCu_3Ti_4O_{12}$ $CaTiO_3$ composite polycrystalline systems. Appl. Phys. Lett. **90**(14), 142912–142913 (2007)
34. Singh, L., Rai, U.S., Mandal, K.D., Sin, B.C., Lee, S.I., Lee, Y.: Dielectric, AC-impedance, modulus studies on $0.5BaTiO_3$ · $0.5CaCu_3Ti_4O_{12}$ nano-composite ceramic synthesized by one-pot, glycine-assisted nitrate-gel route. Ceram. Int. **40**, 10073–10083 (2014)
35. Singh, L., Kim, I.W., Sin, B.C., Woo, S.H., Hyun, S.H., Mandal, K.D., Lee, Y.: Combustion synthesis of nano-crystalline $Bi_{2/3}Cu_3Ti_{2.90}Fe_{0.10}O_{12}$ using inexpensive TiO_2 raw material and its dielectric characterization. Powder Technol. **280**, 256–265 (2015)
36. Khare, A., Yadava, S.S., Gautam, P., Kumar, A., Mandal, K.D., Mukhopadhyay, N.K.: Dielectric properties of nanocomposite based on bismuth copper tianate. J. Aust. Ceram. Soc. **54**(1), 139–147 (2018)
37. Sharma, S., Yadava, S.S., Singh, M.M., Mandal, K.D.: Impedance spectroscopic and dielectric properties of nanosized $Y_{2/3}Cu_3Ti_4O_{12}$ ceramic. J. Adv. Dielectr. **4**(04), 1450030–1450038 (2014)
38. Kannan, Y.B., Saravanan, R., Srinivasan, N., Ismail, I.: Effect of sintering on dielectric and AC conductivity properties of $Ni_{0.5}Zn_{0.5}Fe_2O_4$ nano ferrite particles. J. Aust. Ceram. Soc. **53**(2), 577–581 (2017)
39. Yadava, S.S., Khare, A., Gautam, P., Kumar, A., Mandal, K.D.: Dielectric, ferroelectric and magnetic study of iron doped hexagonal $Ba_4YMn_3O_{11.5-\delta}$ (BYMO) and its dependence on temperature as well as frequency. New J. Chem. **41**(11), 4611–4617 (2017)